Electrochimica Acta 465 (2023) 142994

Contents lists available at ScienceDirect

Electrochimica Acta

journal homepage: www.journals.elsevier.com/electrochimica-acta

Silver hexacyanoferrate (II) nanocrystals as a new material to improve Raman scattering enhancement during silver surface oxidation

Sheila Hernandez [a,*], William Cheuquepan [a,b,c], Martin Perez-Estebanez [a], Aranzazu Heras [a], Alvaro Colina [a,*]

[a] Department of Chemistry, Universidad de Burgos, Pza. Misael Bañuelos s/n, E-09001 Burgos, Spain
[b] Bernal Institute, University of Limerick (UL), Limerick V94 T9PX, Ireland
[c] Department of Chemical Sciences, School of Natural Sciences, University of Limerick (UL), Limerick V94 T9PX, Ireland

ARTICLE INFO

Keywords:
Spectroelectrochemistry
Raman
EC-SERS
EC-SOERS
Electrochemistry

ABSTRACT

Raman spectroscopy is a powerful analysis technique that shows its full potential when a high amplification of the Raman signal is achieved. In this sense, Surface-Enhanced Raman scattering (SERS) has been the most widely used phenomenon for analysis. SERS provides the amplification of the Raman intensity due to the interaction of molecules with a plasmonic nanostructured surface. The enhancement of the Raman signal can be also obtained during the electrochemical oxidation of a metal electrode; this phenomenon was denoted as Electrochemical-Surface Oxidation Enhanced Raman Scattering (EC-SOERS) and yields a good Raman signal enhancement with high reproducibility. Until now, only chloride and bromide have been employed in EC-SOERS, using a silver electrode to generate silver chloride and silver bromide nanocrystals. In this work, a new EC-SOERS substrate based on the electrogeneration of silver hexacyanoferrate (II) nanocrystals is presented which provides a very sensitive Raman response. The electrogeneration of this new material can be easily followed using spectroelectrochemistry since the characteristic Raman bands of the nanocrystals lie outside of the fingerprint region used for the analysis where the detection of most of the target molecules is performed. Indigo Carmine has been selected as target molecule, obtaining a very good response at nanomolar level under Raman resonance and non-resonance conditions.

1. Introduction

Nowadays, the search for new nanomaterials with different chemical, optical or electrical properties is a hot topic. Ferrocyanides, Prussian blue (PB) and analogues have shown excellent optical and electrical properties of interest in several fields, such as plasmonic devices [1], electrocatalysis [2], supercapacitors [3], batteries [4,5], nanomedicine [6,7] and Raman spectroscopy [2,8]. Due to their wide range of applications, the development of new and easy-prepared nanomaterials is of great interest for many researchers in different fields of chemistry and, in particular, in chemical analysis. In this work, silver ferrocyanide nanoparticles are electrochemically generated during the oxidation of a silver electrode with application in the enhancement of the Raman signal for analytical purposes.

Raman spectroscopy is a powerful analytical technique that provides unique vibrational information, which makes it one of the most selective techniques for the identification of compounds. Moreover, with the discovery of *Surface Enhanced Raman Scattering* (SERS) in the mid-1970s, Raman spectroscopy boosted their applications in analysis [9]. Recently, some *in-situ* studies have been published showing the potential of this technique for understanding fundamental reactions of interest in catalysis, surface science and energy science [10–12]. SERS phenomenon can overcome the greatest limitation of Raman spectroscopy, which is the low Raman signal, amplifying the intensity of the scattered light from 3 to 10 orders of magnitude due to the molecule's interaction with a plasmonic nanostructured surface [13–15] or with semiconductor/dielectric nanocrystals [16,17]. The enhancement of the Raman signal is attributed to two different effects: electromagnetic (EM) and chemical (CM) mechanisms. Whereas the first mechanism is associated with the surface plasmon resonance (SPR) of plasmonic structures with light [13,15,18] or with optical resonances in the case of semiconductor/dielectric nanocrystals [16,17], the second one, CM, is attributed to a charge transfer between the molecule and the SERS substrate [13,16,17,19–21]. In the case of metal nanoparticles, it is generally accepted that

* Corresponding authors.
E-mail address: acolina@ubu.es (A. Colina).

https://doi.org/10.1016/j.electacta.2023.142994
Received 2 March 2023; Received in revised form 28 July 2023; Accepted 6 August 2023
Available online 7 August 2023

EM mechanism presents a higher contribution to the enhancement of the Raman signal for metal NPs, presenting an enhancement factor (EF) of 10^5–10^7 [22–24], while the EF attributed to CM is around 10^2–10^3 [19,20,25]. Usually, the EF of the CM in semiconductor/dielectric nanocrystals is higher than in plasmonic nanoparticles [16,17]. The synthesis and structure of these plasmonic NPs are key factors in the Raman response, being able, under some conditions, to detect even a single molecule (SM) [26–28].

Although metallic substrates are typically the most studied in SERS, substrates based on dielectric/semiconductor materials are becoming increasingly popular in recent years [16,29–32]. When dielectric/semiconductors are used as SERS substrates, the CM mechanism has a high impact in the enhancement of the Raman signal due to a charge transfer between the valence band (VB) or the conduction band (CB) of semiconductor and the highest occupied molecular orbital (HOMO) or the lowest unoccupied molecular orbital (LUMO) of the molecule [16]. In contrast, the EM has a low contribution to the EF in semiconductors since the plasmonic band lies in the UV (for VB) or IR region (for CB) of electromagnetic radiation, so no resonance in the visible region is expected. However, some semiconductors have been tuned to exhibit plasmon resonance in the UV–visible [33,34] or NIR [35] region. In any case, different types of optical resonances yield a strong intensification of the local electromagnetic field, contributing to the EM [17]. EF in semiconductors have demonstrated to be almost as effective as metal NPs obtaining EF around 10^5–10^6 [16,36]. The main advantages of these materials are the tunability of the properties [37,38] (by doping or modifying crystal lattice defects), the chemical stability and the low price.

SERS is the most known and commonly used phenomenon in Raman signal enhancement, but not the only one. A few years ago, our research group discovered a new and complementary phenomenon to enhance the Raman scattering during the oxidation of a silver electrode under particular electrolytic conditions, known as *Electrochemical-Surface Oxidation Enhanced Raman Scattering* (EC-SOERS) [39]. This phenomenon has been demonstrated to be highly reproducible [40,41] and analytical enhancement factors higher than 10^5 have been reported [42]. The precipitating agent used, such as chloride or bromide, leads to different nanocrystals with distinct properties, resulting in characteristic Raman responses for different molecules [43] when silver ions are generated by oxidation of the electrode surface.

In this work, potassium ferrocyanide ($K_4[Fe(CN)_6]$) is proposed as a new precipitating agent to obtain a very sensitive EC-SOERS response. The oxidation of a silver electrode, in the presence of $K_4[Fe(CN)_6]$ in acidic medium, produces silver ferrocyanide (AgHCF) nanocrystals deposited on the electrode surface. Further oxidation of the silver electrode yields an enhancement of the Raman scattering. Electrochemical and Raman responses are simultaneously recorded using Time-resolved Raman spectroelectrochemistry (TR-Raman-SEC), obtaining an outstanding enhancement of the Raman signal, higher than usually reported for EC-SOERS.

The new conditions proposed in this work provide a better enhancement of the Raman signal and allow the detection of molecules in nanomolar concentration. Indigo carmine, Fig S1, used as a food colorant in the U.S.A. and E.U. to produce a blue color, has been selected as target molecule and detected under non-resonance and resonance Raman conditions.

2. Experimental section

2.1. Reagents and materials

Indigo carmine (IC, ACROS Organics), perchloric acid ($HClO_4$, 70–72% EMSURE® ACS, ISO, Reag. pH Eur, Merck), potassium hexacyanoferrate (II) ($K_4[Fe(CN)_6]$, HCF, 99+%, ACROS Organics), Potassium hexacyanoferrate (III) ($K_3[Fe(CN)_6]$, 99+%, ACROS Organics), potassium chloride (KCl, 99+%, reagent, ACROS Organics), potassium bromide (KBr, 99+%, reagent, ACROS Organics), silver perchlorate ($AgClO_4$, 99% ACROS Organics). All chemicals were used as received without further purification. Aqueous solutions were freshly prepared using ultrapure water provided by a Milli-Q Direct® purification system (Millipore, 18.2 MΩ cm resistivity at 25 °C and TOC 2 ppb).

2.2. Instrumentation

SEC experiments were performed using two different customized SPELEC-RAMAN instruments (Metrohm-DropSens). One integrates a laser source of 785 nm, and the other one a laser wavelength of 638 nm. Laser power in all experiments was 100 mW (318 Wcm^{-2}) for 785 nm laser source and 20 mW (64 Wcm^{-2}) for the 638 nm laser source. Both instruments have integrated an appropriate spectrometer and a potentiostat. SPELEC DropView software (Metrohm-DropSens) was used for synchronized data acquisition with high temporal resolution, allowing the visualization and analysis of the spectroelectrochemistry data.

Silver screen printed electrodes (AgSPEs) from Metrohm-DropSens (AgSPE, C013) were used as three electrode electrochemical cell in all experiments. These electrodes consist of a silver working electrode of 1.6 mm diameter with a carbon counter electrode and silver paint as a pseudo-reference electrode.

2.3. Spectroelectrochemistry experiments (SEC experiments)

Linear sweep voltammetry (LSV) was selected as electrochemical technique to perform the Raman SEC experiments. The scan rate was fixed at 0.02 $V{\cdot}s^{-1}$ in all experiments and the potential was scanned from −0.10 V to +0.40 V (0.1 M $HClO_4$ + 1 mM $K_4[Fe(CN)_6]$), from −0.05 V to +0.50 V (0.1 M $HClO_4$ + 5 mM KBr) or from 0.00 V to +0.40 V (0.1 M $HClO_4$ + 5 mM KCl). All potentials are referred to the silver pseudo-reference.

All Raman spectra were registered with 1 s of integration time, simultaneously with the electrochemical response.

3. Results and discussion

In this work, a new methodology for the electrochemical synthesis of AgHCF nanoparticles is proposed. The developed method consists of the oxidation of a silver electrode in acidic medium and in presence of a low-concentration potassium hexacyanoferrate (II). This electrochemical-chemical reaction provides well-defined nanocrystals. When a target molecule is present in the analyzed solution using TR-Raman-SEC, the enhancement of its Raman spectrum during the oxidation of the electrode can be observed. This phenomenon, known as EC-SOERS, was reported a few years ago by our research group [39]. Inset in Fig. 1A shows the enhancement of the Raman spectra of IC during a LSV in which a AgHCF SOERS substrate is electrogenerated. LSV is compared with the voltaRamangram at 1524 cm^{-1}, evolution with the applied potential of one of the main bands for IC in Fig. 1A. As can be observed, at +0.25 V, the Raman signal starts to increase, leading to well-defined spectra from this potential onwards (yellow and purple lines in the inset). The inset shows some spectra registered at different potentials: at 0.00 V (blue line), only a peak related to perchlorate is found; at +0.20 V (orange line), the Raman peak related to AgHCF starts to increase, and the perchlorate-related peak keeps constant; at +0.30 V (yellow line) the spectrum shows the Raman peaks for IC and AgHCF; and, finally at +0.40 V (purple line), a very well-defined spectrum for IC and AgHCF is detected because of the enhancement of the substrate. The Raman peaks obtained for IC are in good agreement with those described in literature [44,45] and the band assignment can be found in the Table S1.

The voltammetric response indicates that two processes are taking place during the oxidation of the AgSPE. An anodic peak related to the oxidation of Ag to generate AgHCF ($K_{ps} = 10^{40.8}$) is observed around +0.08 V. After the precipitation, an oxidation current, with an onset around +0.20 V, related to the oxidation of Ag to Ag^+ is observed. These

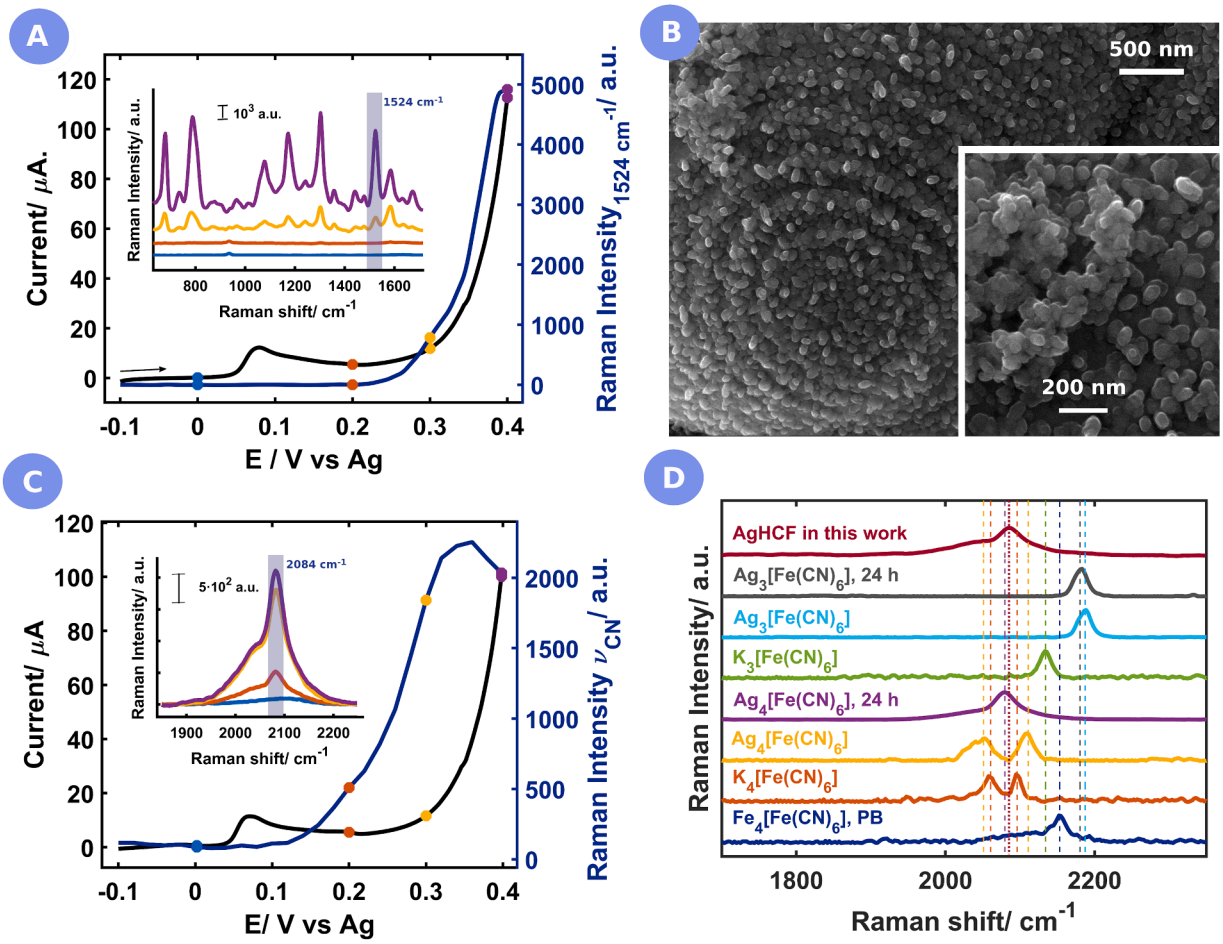

Fig. 1. A) Voltammogram (black line, left axis) compared with VoltaRamangram at 1524 cm^{-1} (blue line, right axis) of 1 μM IC in 1 mM $K_4[Fe(CN)_6]$ and 0.1 M $HClO_4$ on a AgSPE. Inset shows the IC spectra at 0.00 V (blue line), +0.20 V (orange line), +0.30 V (yellow line) and +0.40 V (purple line). **B)** SEM images of AgHCF generated during the SEC experiment with 25000x and 50000x (inset) magnification. The sample was prepared by oxidation of a silver electrode in 1 mM $K_4[Fe(CN)_6]$ and 0.1 M $HClO_4$. **C)** Voltammogram (black solid line, left axis) of 1 mM $K_4[Fe(CN)_6]$ in 0.1 M $HClO_4$ on a AgSPE compared with voltaRamangram at 2084 cm^{-1} (blue line, right axis). The inset shows the ν (CN) spectra at 0.00 V (blue line), +0.20 V (orange line) and +0.40 V (green line). **D)** Comparison of the ν (CN) in the spectra for AgHCF particles generated during the SEC experiment (garnet line), and the spectra of the different possible compounds, from bottom to top: Prussian blue (blue line), potassium ferrocyanide (orange line), silver ferrocyanide (yellow line), silver ferrocyanide after 24 h (crystal, purple line), potassium ferricyanide (green line), silver ferricyanide (pale blue line) and silver ferricyanide after 24 h (crystal, gray line). The potential was scanned from −0.10 V to +0.40 V with a scan rate of 0.02 V s^{-1} for all SEC experiments.

silver ions can also be intercalated into the crystallographic lattice of AgHCF, as was previously described for other HCF and PB analogues [46–49]. It can be seen that the electrochemical response is the same in presence (Fig. 1A) or absence (Fig. 1C) of the target molecule. This behavior demonstrates that the electrochemical processes are only related to the oxidation of the silver electrode and the AgHCF precipitate generation. The surface of the electrode has been studied by Scanning Electron Microscopy (SEM) (Fig. 1B). These images provide information about the shape and size of the generated nanocrystals. Fig. 1B shows SEM images of the electrogenerated AgHCF nanocrystals. A high surface recovery by these agglomerated nanocrystals can be observed, which present homogeneous sizes, finding nanocrystals around 30–50 nm. Some agglomerates of these particles can be appreciated in the inset of Fig. 1B.

The generation and evolution of this material can be followed by TR-Raman-SEC, using a 1 mM $K_4[Fe(CN)_6]$ in 0.1 M $HClO_4$ solution and a AgSPE as Ag^+ source, Fig. 1C. In this case, the Raman response provides valuable information about the material generated on the WE surface, since the AgHCF exhibits a strong Raman band at 2084 cm^{-1} (inset Fig. 1C), corresponding to the stretching mode of cyanide (ν(CN)). The evolution of this peak at 2084 cm^{-1} is plotted versus the applied potential (voltaRamangram, Fig. 1C). After the AgHCF electrochemical generation, the Raman signal at 2084 cm^{-1} starts to increase, reaching a maximum at around +0.37 V. It is noteworthy that the AgHCF Raman peak growth evolves at lower potential than the spectra of the molecule, which suggests a correlation between the electrogeneration of AgHCF particles and the enhancement of the Raman signal.

To identify the material deposited on the WE surface during the first anodic peak in the LSV experiment, Raman spectra of the electrogenerated precipitate have been compared with Raman spectra of chemical synthesized compounds (Fig. 1D). From the literature, it can be expected that mostly $Ag_4[Fe(CN)_6]$ was generated, but the oxidation of this product could lead to $Ag_3[Fe(CN)_6]$ by oxidation of $[Fe^{II}(CN)_6]^{4-}$ to $[Fe^{III}(CN)_6]^{3-}$. Another related compound could be Prussian blue (PB), whose electrochemical generation by redox reactions of ferrocyanide has been reported [50,51].

In order to check and confirm which of these compounds is generated under our experimental conditions, silver ferrocyanide ($Ag_4[Fe(CN)_6]$) and silver ferricyanide ($Ag_3[Fe(CN)_6]$) were chemically synthesized by chemical precipitation, mixing a silver perchlorate and potassium ferro/ferricyanide in equimolar proportions. The precipitated product was rinsed with water and separated by centrifugation. This washing procedure was repeated three times. These products were labelled in Fig. 1D as "$Ag_4[Fe(CN)_6]$" (yellow line) and "$Ag_3[Fe(CN)_6]$" (pale blue). The

obtained products were then dispersed in water and aged for 24 h to lead to bigger crystals, labelled as "$Ag_4[Fe(CN)_6]$, 24 h" (purple line) and "$Ag_3[Fe(CN)_6]$, 24 h" (gray line). Besides, commercial samples of PB (blue line), potassium ferrocyanide (orange line) and potassium ferricyanide (blue line) were analyzed, and the corresponding Raman spectra were compared with the ones obtained under our electrolytic conditions in Fig. 1C. From the different spectra in this figure, the electrochemically generated AgHCF seems to be crystalline $Ag_4[Fe(CN)_6]$ because of the clear matching of the two spectra and the difference with the others. The clear difference between the $Ag_4[Fe(CN)_6]$ and $Ag_4[Fe(CN)_6]$, 24 h spectra indicates that, for this compound, the electrochemical generation directly yields a crystal lattice like the aged precipitate.

The role of the potential in the evolution of the Raman enhancement is undoubtedly very interesting for understanding EC-SOERS. A AgHCF substrate was generated by performing a LSV from −0.10 V to +0.40 V with a scan rate of 0.02 V s^{-1} in a 1 mM $K_4[Fe(CN)_6]$ and 0.1 M $HClO_4$ solution. Once the AgHCF substrate was generated, it was thoroughly rinsed with deionized water and a 0.1 M $HClO_4$ solution. Then, a 1 μM IC + 0.1 M $HClO_4$ was added on the substrate, obtaining the spectrum (garnet line) shown in Fig. 2, where no Raman bands were observed, demonstrating that the substrate is not active when only the molecule is added on the substrate. However, when a solution containing 1 μM IC + 0.01 M Ag^+ + 0.1 M $HClO_4$ was added on the substrate, the spectrum (green line) of IC was clearly defined as can be shown in Fig. 2, demonstrating the enhancement of the SOERS substrate. Therefore, the role of potential is the generation of Ag cations which activate the SOERS substrate.

The use of AgHCF as substrate for Raman enhancement presents some advantages, such as low spectroscopic interference with adsorbed molecules. AgHCF only shows Raman peaks in the silent region (gray zone in Fig. S2, 1800–2800 cm^{-1}) and small interferences in the region below 600 cm^{-1} (blue zone, Fig. S2), while no bands are observed in the typical fingerprint region of most molecules (green zone, Fig. S2, 600–1800 cm^{-1}), like other similar HCFs and PBs [8]. This fact allows the simultaneous assessment of substrate generation and molecule detection.

This new substrate allows the detection of IC with good sensitivity, obtaining clearly defined signals even at micromolar range (orange line, Fig. S2). However, the sensitivity of the method for IC detection can be further improved with additional Raman enhanced phenomena, such as Raman resonance (RR), which can be observed under specific laser wavelengths (Fig. S3) as has been reported in the literature [44,52]. In this work, the main laser source employed is 785 nm, so it should not be

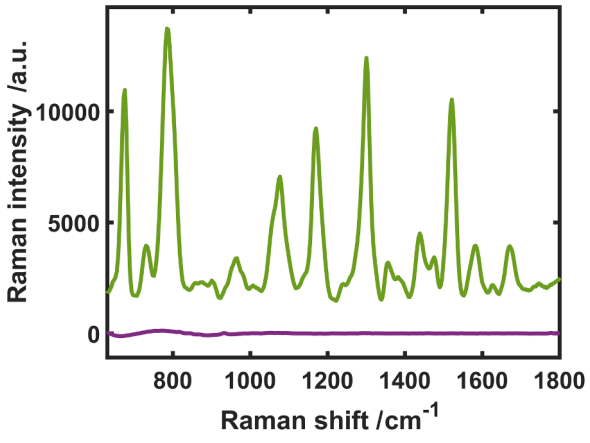

Fig. 2. Raman spectrum corresponding to a 1 μM IC + 0.1 M $HClO_4$ solution added on the AgHCF substrate generated on a AgSPE (garnet line) and a 1 μM IC + 0.05 M Ag^+ + 0.1 M $HClO_4$ solution added on the AgHCF substrate generated on a AgSPE (green line).

expected a RR process using this laser source (red line, Fig. S3). However, a laser source with a shorter wavelength can be used to improve the sensitivity and the limit of detection (LOD); in our case, a 638 nm laser source presents RR (orange line, Fig. S3). Concentrations as low as 10 nM can be detected using this laser (green lines, Fig. 2B and 2D).

To evaluate the performance of AgHCF as EC-SOERS substrate, the IC Raman response was evaluated for three different precipitating agents: 5 mM KBr, 5 mM KCl and 1 mM HCF. All solutions were freshly prepared in 0.1 M $HClO_4$ as supporting electrolyte.

Fig. 3A shows the Raman spectra for a high concentration of IC, between 1 and 100 μM. No Raman response is obtained when using KBr (blue line), indicating that the generated structures based on KBr do not yield an enhancement of the Raman signal for IC. The other well-known precipitant used in EC-SOERS is KCl. In this case, a 100 μM IC solution in this electrolytic medium is tested (purple line), obtaining a good response. However, a much more sensitive Raman response is observed using $K_4[Fe(CN)_6]$ as precipitating agent (garnet line), obtaining a higher signal with a concentration 100 times lower. Lower concentrations of IC are represented in Fig. 3B. In this case, only KCl and $K_4[Fe(CN)_6]$ were employed as precipitating agents, since KBr substrates did not show any Raman enhancement for this molecule. A 10 μM IC solution was tested in KCl showing a low intensity but defined spectrum. As was expected, a better response is obtained for $K_4[Fe(CN)_6]$, being able to detect a concentration as low as 50 nM. When the sample was studied under resonance conditions (638 nm laser source), lower concentrations could be detected 10 nM (Fig. 2B, green line). This spectrum, however, shows a better response for 1585 cm^{-1} peak. For this reason, this peak is the one represented versus the applied potential in the VoltaRamangram (Fig. 2D, green dotted line). The evolution of these spectra with potential is illustrated in Fig. 2C and Fig. 2D. These figures show the comparison between the LSV for each experiment (solid line, left axis) and the voltaRamangram at 1524 cm^{-1} (non-resonance, blue, garnet and purple dotted lines) or 1585 cm^{-1} (RR, green dotted line). The inset shows the VoltaRamangrams for 10 μM IC in KBr (inset in Fig. 2C) and 10 μM IC in KCl (inset in Fig. 2D). Orange line represents the limit of detection (3σ, three times the standard deviation) [53], confirming that there is no signal at all for IC in KBr, while the peak for 10 μM IC in KCl is, unequivocally, a band of the molecule that can be easily distinguished from noise.

One of the main advantages of SEC techniques is that they provide dynamic information about the studied system since the evolution of the Raman spectra with the applied potential can be followed. Thanks to this, it is possible to identify the detector's electronic noise signal in a given experiment, since the sample presents a range of potentials where no signal is found, which coincides with the potential region in which the appropriate substrate has not been generated to detect that molecule. A clear noise evolution is obtained during the first part of the LSV, where any molecule is detected. This is a clear advantage of TR-Raman-SEC with respect to a simple Raman experiment.

In order to compare the different substrates, the enhancement factor (EF) obtained for IC under different electrolytic conditions described above was assessed. However, since the substrate is changing due to the applied potential during the SEC experiment, it is very challenging to determine the number of molecules adsorbed on the substrate and, therefore, it is not feasible to obtain the EF. A good alternative is to calculate the analytical enhancement factor (AEF) [54,55] in which only the concentration of the molecule in solution is considered, and the obtained Raman intensity is compared with the one obtained for the molecule in absence of an EC-SOERS substrate. An ordinary Raman spectrum of 0.5 mM IC (in water) was measured to assess the AEF, according to Eq. S1, yielding an AEF of $3{\cdot}10^2$ for KCl (0.1 mM IC, 0.1 M $HClO_4$, 5 mM KCl) and an AEF of $4{\cdot}10^4$ for HCF (1 μM IC, 0.1 M $HClO_4$, 1 mM $K_4[Fe(CN)_6]$). For more information about the AEF calculation, see the S4 section in the Supplementary Material. These results show an improvement of two orders of magnitude of the EC-SOERS substrate for IC in an electrolytic medium with HCF, where AgHCF is generated. This

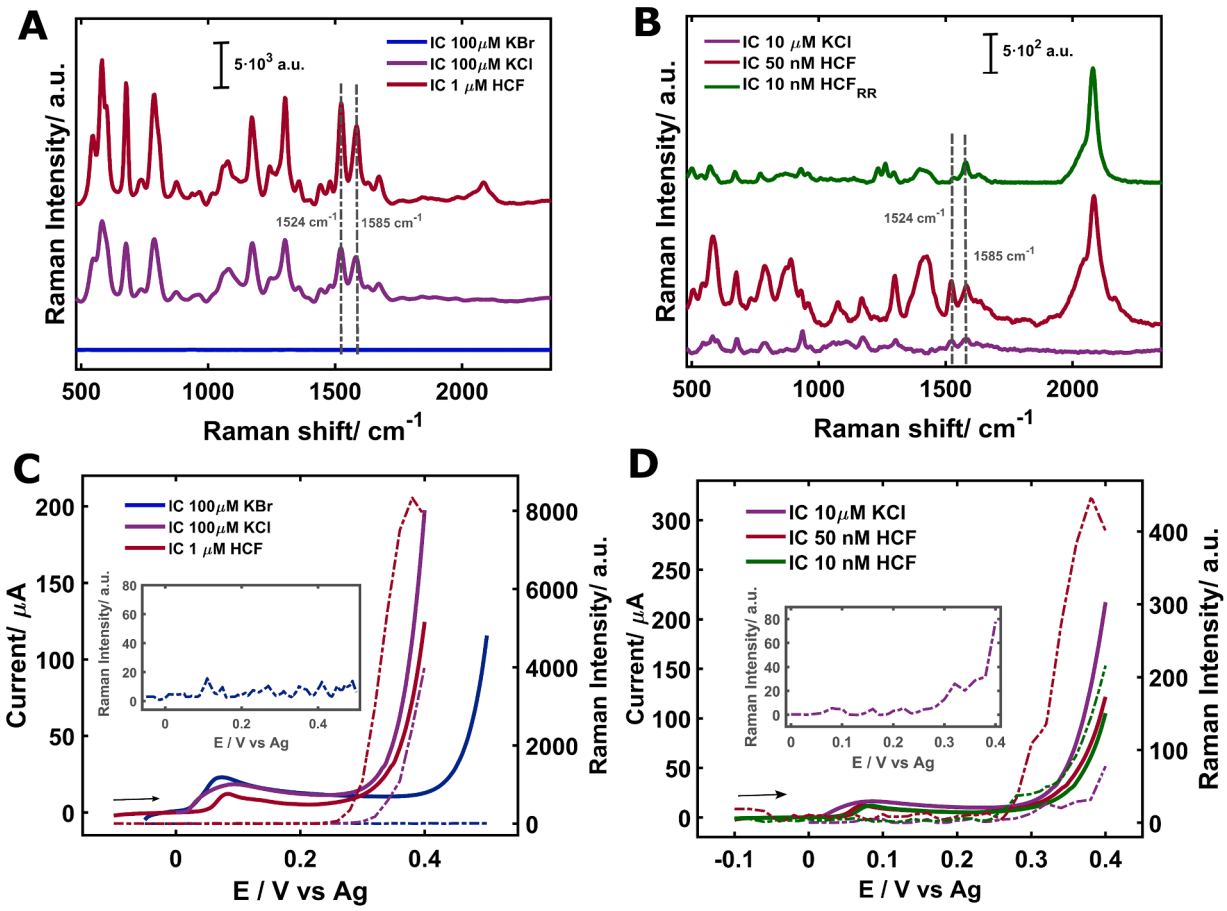

Fig. 3. Results for different IC concentrations and different precipitating agents are presented, all with 0.1 M $HClO_4$. **A)** Comparison between spectra taken at the oxidation vertex potential for 100 μM IC in 5 mM KCl (purple line) and 5 mM KBr (blue line) and 1 μM IC in 1 mM $K_4[Fe(CN)_6]$ (garnet line). **B)** Spectra taken near the LOD, 10 μM IC in KCl (purple line), 50 nM in $K_4[Fe(CN)_6]$ (garnet line) and 10 nM in $K_4[Fe(CN)_6]$ with Raman resonance (RR, green line). **C)** and **D)** show a comparison of the voltammogram (solid lines) and voltaRamangram (dotted lines) for the principal peak in each experiment (1524 cm^{-1} for all, except for Raman Resonance experiment, green line, where the peak at 1580 cm^{-1} is chosen).

improvement is also demonstrated for uric acid (UA), which presents an AEF of around 10^4 for KCl versus 10^6 for HCF. In contrast, caffeine, for example, shows an EC-SOERS response in KCl and KBr [43] but no Raman response in HCF (data not shown). The differences in the enhancement factors are probably due to the different interactions between the molecule and the Ag/AgHCF/Ag^+ substrate, with molecules such as IC or UA interacting more favorably with AgHCF/Ag^+ crystal nanoparticles.

One of the advantages of AgHCF substrates is the capability of detection of different molecules. As an example, Fig S5 shows the spectroelectrochemical signals corresponding to four different molecules (5 μM alizarin red S, 10 μM ponceau4R, 10 μM bromophenol blue and 10 μM riboflavin) obtained during a LSV. Potential was scanned from −0.10 V to +0.40 V at a scan rate of 0.02 V s^{-1} in a 1 mM $K_4[Fe(CN)_6]$ and 0.1 M $HClO_4$ solution, containing the target molecule. All the experiments were performed in a AgSPE. As can be observed, similar voltammograms, Fig S5A, are recorded for the four analytes, indicating that a similar EC-SOERS substrate is obtained in all cases. However, the enhancement of the Raman signal is different for each analyte. For analysis, the experimental conditions have to be optimized for the target analyte. In all cases, a clear voltaRamangram, Fig S5A, is observed during the oxidation of the Ag/AgHCF electrode, obtaining well-defined Raman spectra at the oxidation vertex potential, Fig S5B.

The new AgHCF substrates for EC-SOERS are very sensitive, providing, to the best of our knowledge, the highest EF reported for SOERS to date. For analytical applications, not only sensitivity but also reproducibility is very important. Up to now, potential controlled experiments provide very sensitive substrates with a reproducibility typical of SERS, around 20% of relative standard deviation (RSD) [13]. More reproducible experiments can be obtained using galvanostatic strategies. Fig. 4 shows the VoltaRamangrams of five experiments

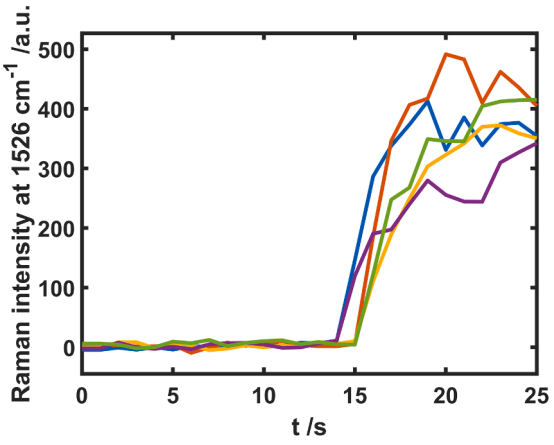

Fig. 4. VoltaRamangrams at 1524 cm^{-1} corresponding to five galvanostatic experiments obtained by applying a current of +5 μA for 15 s and +100 μA for 10 s in a 500 nM IC + 1 mM $K_4[Fe(CN)_6]$ + 0.1 M $HClO_4$ solution using a AgSPE.

performed by applying a current of +5 μA for 15 s to generate the AgHCF nanocrystals and a subsequent +100 μA current for 10 s to generate Ag cations in order to activate the SOERS substrate. The experiments are performed in a 500 nM IC+ 1 mM $K_4[Fe(CN)_6]$ + 0.1 M $HClO_4$ solution, using a AgSPE. As can be seen, responses with good reproducibility are obtained, showing a 9% of RSD at $t = 25$ s, demonstrating the good capability of EC-SOERS methodology for analysis in a very short time and using a small sample volume, only 50 μL. Optimization of the experimental conditions is mandatory for obtaining EC-SOERS substrates for analytical purposes. This work opens new gates for designing Raman-SEC experiments for the detection of molecules at trace level.

4. Conclusion

A new precipitating agent, potassium hexacyanoferrate (II), has been used in this work to obtain EC-SOERS responses during a TR-Raman-SEC experiment. $K_4[Fe(CN)_6]$ induces the generation of $Ag_4[Fe(CN)_6]$ (AgHCF) polydisperse nanocrystals, as has been deduced from the Raman spectra and the SEM images.

$K_4[Fe(CN)_6]$ presents advantages over other precipitating agents such as KCl or KBr. On the one hand, the Raman bands related to AgHCF are present in the silent region for most molecules providing a substrate with no interferences, allowing a simultaneous study of the substrate and the analyte. On the other hand, a more sensitive Raman response is obtained using this electrolyte medium for certain molecules such as IC or UA.

IC has been selected as test molecule to compare the different electrolytic conditions. $K_4[Fe(CN)_6]$ has proven to provide greater enhancement of this analyte than KBr or KCl. Concentration as low as 50 nM can be detected using this precipitating agent, under non-resonant conditions, but this signal can be improved by tuning up the laser wavelength to promote Raman Resonance, enabling the detection of 10 nM IC. The limit of detection can be easily found during the experiment, using the voltaRamangram, calculating three times the standard deviation (3σ) in the zone where no signal is expected, being able of clearly differentiate between noise and signal.

Finally, the AEFs for IC and UA are presented using $K_4[Fe(CN)_6]$ or KCl as precipitating agent. It is found that $K_4[Fe(CN)_6]$ provides AEF two orders of magnitude higher than KCl for the studied conditions. This difference can be attributed to the interaction between the analytes and $AgHCF/Ag^+$ crystal particles, which seems highly promoted, favoring a nanocrystal-molecule charge transfer and providing a more significant amplification of the Raman signal at anodic potentials using silver electrodes.

Credit author statement

S. H. and M.P.E. contributed to the acquisition of data. S.H, W.Ch, M. P-E, A.H and A.C. contributed to the conception, design and implementation of the research and to the analysis and interpretation of the results. S.H, W.Ch, M.P-E, A.H and A.C. contributed to the writing of the manuscript and to the revision of the manuscript critically for important intellectual content. This work has been headed by A.C. and S.H.

Declaration of Competing Interest

The authors declare that they have no known competing financial interests or personal relationships that could have appeared to influence the work reported in this paper.

Data availability

Data will be available at the Universidad de Burgos data repository

Acknowledgements

Authors acknowledge the financial support from Ministerio de Ciencia e Innovación and Agencia Estatal de Investigación (MCIN/AEI/10.13039/501100011033, PID2020–113154RB-C21), and Ministerio de Ciencia, Innovación y Universidades (RED2022–134120-T). S.H. thanks JCyL and European Social Fund for her postdoctoral fellowship and M. P.-E. thanks JCyL and European Social Fund for his predoctoral fellowship. W. Ch. acknowledges Junta de Castilla y León for his postdoctoral fellowship (Grant BU297P18) and funding received from European Union's Horizon 2020 research and innovation program under the Marie Skłodowska-Curie grant agreement No 101031622.

Supplementary materials

Supplementary material associated with this article can be found, in the online version, at doi:10.1016/j.electacta.2023.142994.

References

[1] Y.Q. Liu, W. Zhu, J.M. Hu, A.G. Shen, Recent advances in plasmonic Prussian blue-based SERS nanotags for biological application, Nanoscale Adv. 3 (2021) 6568–6579, https://doi.org/10.1039/d1na00464f.
[2] R. Mažeikien, G. Niaura, A. Malinauskas, Electrocatalytic reduction of hydrogen peroxide at Prussian blue modified electrode: an in situ Raman spectroelectrochemical study, J. Electroanal. Chem. 660 (2011) 140–146, https://doi.org/10.1016/j.jelechem.2011.06.022.
[3] J. Chen, K. Huang, S. Liu, Insoluble metal hexacyanoferrates as supercapacitor electrodes, Electrochem. Commun. 10 (2008) 1851–1855, https://doi.org/10.1016/j.elecom.2008.07.046.
[4] K. Hurlbutt, S. Wheeler, I. Capone, M. Pasta, Prussian Blue Analogs as Battery Materials, Joule. 2 (2018) 1950–1960. doi:10.1016/j.joule.2018.07.017.
[5] C.D. Wessells, R.A. Huggins, Y. Cui, Copper hexacyanoferrate battery electrodes with long cycle life and high power, Nat. Commun. 2 (2011) 2–6, https://doi.org/10.1038/ncomms1563.
[6] S. Mukherjee, R. Kotcherlakota, S. Haque, S. Das, S. Nuthi, D. Bhattacharya, K. Madhusudana, S. Chakravarty, R. Sistla, C.R. Patra, Silver Prussian Blue Analogue Nanoparticles: rationally Designed Advanced Nanomedicine for Multifunctional Biomedical Applications, ACS Biomater. Sci. Eng. 6 (2020) 690–704, https://doi.org/10.1021/acsbiomaterials.9b01693.
[7] C.R. Patra, Prussian blue nanoparticles and their analogues for application to cancer theranostics, Nanomedicine 11 (2016) 569–572, https://doi.org/10.2217/nnm.16.16.
[8] Y. Yin, Q. Li, S. Ma, H. Liu, B. Dong, J. Yang, D. Liu, Prussian Blue as a Highly Sensitive and Background-Free Resonant Raman Reporter, Anal. Chem. 89 (2017) 1551–1557, https://doi.org/10.1021/acs.analchem.6b03521.
[9] M. Fleischmann, P.J.J. Hendra, A.J.J. McQuillan, Raman spectra of pyridine adsorbed at a silver electrode, Chem. Phys. Lett. 26 (1974) 163–166, https://doi.org/10.1016/0009-2614(74)85388-1.
[10] Y.H. Wang, S. Zheng, W.M. Yang, R.Y. Zhou, Q.F. He, P. Radjenovic, J.C. Dong, S. Li, J. Zheng, Z.L. Yang, G. Attard, F. Pan, Z.Q. Tian, J.F. Li, In situ Raman spectroscopy reveals the structure and dissociation of interfacial water, Nature. 600 (2021) 81–85. doi:10.1038/s41586-021-04068-z.
[11] A. Goyal, M.T.M. Koper, The Interrelated Effect of Cations and Electrolyte pH on the Hydrogen Evolution Reaction on Gold Electrodes in Alkaline Media, Angew. Chemie Int. Ed. 60 (2021) 13452–13462, https://doi.org/10.1002/anie.202102803.
[12] M. Moradzaman, G. Mul, In Situ Raman Study of Potential-Dependent Surface Adsorbed Carbonate, CO, OH, and C Species on Cu Electrodes During Electrochemical Reduction of CO 2, ChemElectroChem. 8 (2021) 1478–1485. doi:10.1002/celc.202001598.
[13] J. Langer, D.J. de Aberasturi, J. Aizpurua, R.A. Alvarez-Puebla, B. Auguié, J. J. Baumberg, G.C. Bazan, S.E.J. Bell, A. Boisen, A.G. Brolo, J. Choo, D. Cialla-May, V. Deckert, L. Fabris, K. Faulds, F.Javier García de Abajo, R. Goodacre, D. Graham, A.J. Haes, C.L. Haynes, C. Huck, T. Itoh, M. Käll, J. Kneipp, N.A. Kotov, H. Kuang, E.C. Le Ru, H.K. Lee, J.F. Li, X.Y. Ling, S.A. Maier, T. Mayerhöfer, M. Moskovits, K. Murakoshi, J.M. Nam, S. Nie, Y. Ozaki, I. Pastoriza-Santos, J. Perez-Juste, J. Popp, A. Pucci, S. Reich, B. Ren, G.C. Schatz, T. Shegai, S. Schlücker, L.L. Tay, K. George Thomas, Z.Q. Tian, R.P. van Duyne, T. Vo-Dinh, Y. Wang, K.A. Willets, C. Xu, H. Xu, Y. Xu, Y.S. Yamamoto, B. Zhao, L.M. Liz-Marzán, Present and future of surface-enhanced Raman scattering, ACS Nano 14 (2020) 28–117, https://doi.org/10.1021/acsnano.9b04224.
[14] P.L. Stiles, J.A. Dieringer, N.C. Shah, R.P. Van Duyne, Surface-Enhanced Raman Spectroscopy, Annu. Rev. Anal. Chem. 1 (2008) 601–626, https://doi.org/10.1146/annurev.anchem.1.031207.112814.
[15] S. Schlücker, Surface-Enhanced Raman Spectroscopy: concepts and Chemical Applications, Angew. Chemie Int. Ed. 53 (2014) 4756–4795, https://doi.org/10.1002/anie.201205748.

[16] J.R. Lombardi, R.L. Birke, Theory of surface-enhanced raman scattering in semiconductors, J. Phys. Chem. C. 118 (2014) 11120–11130, https://doi.org/10.1021/jp5020675.
[17] I. Alessandri, J.R. Lombardi, Enhanced Raman Scattering with Dielectrics, Chem. Rev. 116 (2016) 14921–14981, https://doi.org/10.1021/acs.chemrev.6b00365.
[18] D.Y. Wu, J.F. Li, B. Ren, Z. Tian, Electrochemical surface-enhanced Raman spectroscopy of nanostructures, Chem. Soc. Rev. 37 (2008) 1025, https://doi.org/10.1039/b707872m.
[19] A. Campion, J.E.E. Ivanecky, C.M.M. Child, M. Foster, On the Mechanism of Chemical Enhancement in Surface-Enhanced Raman Scattering, J. Am. Chem. Soc. 117 (1995) 11807–11808, https://doi.org/10.1021/ja00152a024.
[20] P. Kambhampati, C.M. Child, M.C. Foster, A. Campion, On the chemical mechanism of surface enhanced Raman scattering: experiment and theory, J. Chem. Phys. 108 (1998) 5013–5026, https://doi.org/10.1063/1.475909.
[21] S.J. Lee, Z. Guan, H. Xu, M. Moskovits, Surface-enhanced Raman spectroscopy and nanogeometry: the plasmonic origin of SERS, J. Phys. Chem. C. 111 (2007) 17985–17988, https://doi.org/10.1021/jp077422g.
[22] S.Y. Ding, E.M. You, Z.Q. Tian, M. Moskovits, Electromagnetic theories of surface-enhanced Raman spectroscopy, Chem. Soc. Rev. 46 (2017) 4042–4076, https://doi.org/10.1039/C7CS00238F.
[23] S.Y. Ding, J. Yi, J.F. Li, B. Ren, D.Y. Wu, R. Panneerselvam, Z.Q. Tian, Nanostructure-based plasmon-enhanced Raman spectroscopy for surface analysis of materials, Nat. Rev. Mater. 1 (2016) 16021–16036, https://doi.org/10.1038/natrevmats.2016.21.
[24] J.A. Dieringer, A.D. McFarland, N.C. Shah, D.A. Stuart, A.V. Whitney, C.R. Yonzon, M.A. Young, X. Zhang, R.P. Van Duyne, Surface enhanced Raman spectroscopy: new materials, concepts, characterization tools, and applications, Faraday Discuss 132 (2006) 9–26, https://doi.org/10.1039/b513431p.
[25] N. Valley, N. Greeneltch, R.P. Van Duyne, G.C. Schatz, A look at the origin and magnitude of the chemical contribution to the enhancement mechanism of surface-enhanced Raman spectroscopy (SERS): theory and experiment, J. Phys. Chem. Lett. 4 (2013) 2599–2604, https://doi.org/10.1021/jz4012383.
[26] S.L. Kleinman, E. Ringe, N. Valley, K.L. Wustholz, E. Phillips, K.A. Scheidt, G. C. Schatz, R.P. Van Duyne, Single-molecule surface-enhanced raman spectroscopy of crystal violet isotopologues: theory and experiment, J. Am. Chem. Soc. 133 (2011) 4115–4122, https://doi.org/10.1021/ja110964d.
[27] K. Kneipp, Y. Wang, H. Kneipp, L.T. Perelman, I. Itzkan, R.R. Dasari, M.S. Feld, Single Molecule Detection Using Surface-Enhanced Raman Scattering (SERS), Phys. Rev. Lett. 78 (1997) 1667–1670, https://doi.org/10.1103/PhysRevLett.78.1667.
[28] D. Martín-Yerga, A. Pérez-Junquera, M.B. González-García, D. Hernández-Santos, P. Fanjul-Bolado, Towards single-molecule in situ electrochemical SERS detection with disposable substrates, Chem. Commun. 54 (2018) 5748–5751, https://doi.org/10.1039/C8CC02069H.
[29] Y. Peng, C. Lin, L. Long, T. Masaki, M. Tang, L. Yang, J. Liu, Z. Huang, Z. Li, X. Luo, J.R. Lombardi, Y. Yang, Charge-Transfer Resonance and Electromagnetic Enhancement Synergistically Enabling MXenes with Excellent SERS Sensitivity for SARS-CoV-2 S Protein Detection, Nano-Micro Lett. 13 (2021) 1–17, https://doi.org/10.1007/s40820-020-00565-4.
[30] Z. Mao, W. Song, L. Chen, W. Ji, X. Xue, W. Ruan, Z. Li, H. Mao, S. Ma, J. R. Lombardi, B. Zhao, Metal-semiconductor contacts induce the charge-transfer mechanism of surface-enhanced raman scattering, J. Phys. Chem. C. 115 (2011) 18378–18383, https://doi.org/10.1021/jp206455a.
[31] B. Yang, S. Jin, S. Guo, Y. Park, L. Chen, B. Zhao, Y.M. Jung, Recent Development of SERS Technology: semiconductor-Based Study, ACS Omega 4 (2019) 20101–20108, https://doi.org/10.1021/acsomega.9b03154.
[32] G. Demirel, H. Usta, M. Yilmaz, M. Celik, H.A. Alidagi, F. Buyukserin, Surface-enhanced Raman spectroscopy (SERS): an adventure from plasmonic metals to organic semiconductors as SERS platforms, J. Mater. Chem. C. 6 (2018) 5314–5335, https://doi.org/10.1039/C8TC01168K.
[33] D. Maznichenko, K. Venkatakrishnan, B. Tan, Stimulating multiple SERS mechanisms by a nanofibrous three-dimensional network structure of titanium dioxide (TiO2), J. Phys. Chem. C. 117 (2013) 578–583, https://doi.org/10.1021/jp310193a.
[34] X.X. Han, W. Ji, B. Zhao, Y. Ozaki, Semiconductor-enhanced Raman scattering: active nanomaterials and applications, Nanoscale. 9 (2017) 4847–4861. doi:10.1039/c6nr08693d.
[35] J.M. Luther, P.K. Jain, T. Ewers, A.P. Alivisatos, Localized surface plasmon resonances arising from free carriers in doped quantum dots, Nat. Mater. 10 (2011) 361–366, https://doi.org/10.1038/nmat3004.
[36] X. Wang, W. Shi, S. Wang, H. Zhao, J. Lin, Z. Yang, M. Chen, L. Guo, Two-Dimensional Amorphous TiO2 Nanosheets Enabling High-Efficiency Photoinduced Charge Transfer for Excellent SERS Activity, J. Am. Chem. Soc. 141 (2019) 5856–5862, https://doi.org/10.1021/jacs.9b00029.
[37] C. Zhou, L. Sun, F. Zhang, C. Gu, S. Zeng, T. Jiang, X. Shen, D.S. Ang, J. Zhou, Electrical tuning of the sers enhancement by precise defect density control, ACS Appl. Mater. Interfaces 11 (2019) 34091–34099, https://doi.org/10.1021/acsami.9b10856.
[38] J. Lin, Y. Shang, X. Li, J. Yu, X. Wang, L. Guo, Ultrasensitive SERS Detection by Defect Engineering on Single Cu2O Superstructure Particle, Adv. Mater. (2017) 29, https://doi.org/10.1002/adma.201604797.
[39] J.V. Perales-Rondon, S. Hernandez, D. Martin-Yerga, P. Fanjul-Bolado, A. Heras, A. Colina, Electrochemical surface oxidation enhanced Raman scattering, Electrochim. Acta. 282 (2018) 377–383, https://doi.org/10.1016/j.electacta.2018.06.079.
[40] S. Hernandez, J.V. Perales-Rondon, A. Heras, A. Colina, Determination of uric acid in synthetic urine by using electrochemical surface oxidation enhanced Raman scattering, Anal. Chim. Acta. 1085 (2019) 61–67, https://doi.org/10.1016/j.aca.2019.07.057.
[41] S. Hernandez, J.V. Perales-Rondon, A. Heras, A. Colina, Electrochemical SERS and SOERS in a single experiment: a new methodology for quantitative analysis, Electrochim. Acta. 334 (2020), 135561, https://doi.org/10.1016/j.electacta.2019.135561.
[42] S. Hernandez, J.V. Perales-Rondon, A. Heras, A. Colina, Enhancement factors in electrochemical surface oxidation enhanced Raman scattering, Electrochim. Acta. 380 (2021), 138223, https://doi.org/10.1016/j.electacta.2021.138223.
[43] M. Perez-Estebanez, S. Hernandez, J.V. Perales-Rondon, E. Gomez, A. Heras, A. Colina, Chemical selectivity in electrochemical surface oxidation enhanced Raman scattering, Electrochim. Acta. 353 (2020), 136560, https://doi.org/10.1016/j.electacta.2020.136560.
[44] N. Peica, W. Kiefer, Characterization of indigo carmine with surface-enhanced resonance Raman spectroscopy (SERRS) using silver colloids and island films, and theoretical calculations, J. Raman Spectrosc. 39 (2008) 47–60, https://doi.org/10.1002/jrs.1813.
[45] I.T. Shadi, B.Z. Chowdhry, M.J. Snowden, R. Withnall, Semi-quantitative analysis of indigo carmine, using silver colloids, by surface enhanced resonance Raman spectroscopy (SERRS), Spectrochim. Acta - Part A Mol. Biomol. Spectrosc. 59 (2003) 2201–2206, https://doi.org/10.1016/S1386-1425(03)00063-5.
[46] J. Nai, X.W. Lou, Hollow Structures Based on Prussian Blue and Its Analogs for Electrochemical Energy Storage and Conversion, Adv. Mater. 31 (2019) 1–20, https://doi.org/10.1002/adma.201706825.
[47] B. Wang, S. Liu, W. Sun, Y. Tang, H. Pan, M. Yan, Y. Jiang, Intercalation Pseudocapacitance Boosting Ultrafast Sodium Storage in Prussian Blue Analogs, ChemSusChem 12 (2019) 2415–2420, https://doi.org/10.1002/cssc.201900582.
[48] Y. Moritomo, M. Takachi, Y. Kurihara, T. Matsuda, Synchrotron-radiation X-ray investigation of Li+/Na+ intercalation into Prussian blue analogues, Adv. Mater. Sci. Eng. (2013) 2013, https://doi.org/10.1155/2013/967285.
[49] H. Zhang, Q. Jiang, J.H.L. Hadden, F. Xie, D.J. Riley, Pd Ion-Exchange and Ammonia Etching of a Prussian Blue Analogue to Produce a High-Performance Water-Splitting Catalyst, Adv. Funct. Mater. 31 (2021), 2008989, https://doi.org/10.1002/adfm.202008989.
[50] A. Heras, A. Colina, V. Ruiz, J. López-Palacios, UV-visible spectroelectrochemical detection of side-reactions in the hexacyanoferrate(III)/(II) electrode process, Electroanalysis 15 (2003) 702–708, https://doi.org/10.1002/elan.200390088.
[51] J. López-Palacios, A. Heras, Á. Colina, V. Ruiz, Bidimensional spectroelectrochemical study on electrogeneration of soluble Prussian Blue from hexacyanoferrate(II) solutions, Electrochim. Acta. 49 (2004) 1027–1033, https://doi.org/10.1016/j.electacta.2003.10.013.
[52] A. Dhara, A. Baral, S. Chabri, A. Sinha, N.R. Bandyopadhyay, N. Mukherjee, An Efficient Approach Towards the Photodegradation of Indigo Carmine by Introducing ZnO/CuO/Si Ternary Nanocomposite as Photocatalyst, J. Inst. Eng. Ser. D. 98 (2017) 1–8, https://doi.org/10.1007/s40033-016-0111-2.
[53] G.L. Long, J.D. Winefordner, Limit of Detection A Closer Look at the IUPAC Definition, Anal. Chem. 55 (1983) 712A–724A, https://doi.org/10.1021/ac00258a724.
[54] E.C. Le Ru, E. Blackie, M. Meyer, P.G. Etchegoin, Surface Enhanced Raman Scattering Enhancement Factors: a Comprehensive Study, J. Phys. Chem. C. 111 (2007) 13794–13803, https://doi.org/10.1021/jp0687908.
[55] I.E. Pavel, K.S. Alnajjar, J.L. Monahan, A. Stahler, N.E. Hunter, K.M. Weaver, J. D. Baker, A.J. Meyerhoefer, D.A. Dolson, Estimating the analytical and surface enhancement factors in surface-enhanced raman scattering (SERS): a novel physical chemistry and nanotechnology laboratory experiment, J. Chem. Educ. 89 (2012) 286–290, https://doi.org/10.1021/ed200156n.